International Journal of Nanomedicine

Dovepress
Taylor & Francis Group

Open Access Full Text Article

ORIGINAL RESEARCH

Combined Esculentin-2CHa Fusion Protein-Coated Au Nanoparticles for Effective Against Non-Alcoholic Fatty Liver Disease in Mice Model

Reeju Amatya[1], Amala Joseph[1], Gu Seob Roh[2], Cheol Moon[3], Yassmine Benmokadem[4], Doyeon Kim[4], Kyoung Ah Min[4], Meong Cheol Shin[1]

[1]College of Pharmacy and Research Institute of Pharmaceutical Sciences, Gyeongsang National University, Jinju, Gyeongnam, 52828, Republic of Korea; [2]Department of Anatomy and Convergence Medical Science, Metabolic Dysfunction Liver Disease Research Center, Institute of Medical Science, College of Medicine, Gyeongsang National University, Jinju, Gyeongnam, 52727, Republic of Korea; [3]College of Pharmacy and Research Institute of Life and Pharmaceutical Sciences, Sunchon National University, Suncheon, Jeonnam, 57922, Republic of Korea; [4]College of Pharmacy and Inje Institute of Pharmaceutical Sciences and Research, Inje University, Gimhae, Gyeongnam, 50834, Republic of Korea

Correspondence: Meong Cheol Shin, College of Pharmacy and Research Institute of Pharmaceutical Sciences, Gyeongsang National University, Jinju, Gyeongnam, 52828, Republic of Korea, Tel +1 82 55 772 2421, Fax +1 82 55 772 2429, Email shinmc@gnu.ac.kr; Kyoung Ah Min, College of Pharmacy and Inje Institute of Pharmaceutical Sciences and Research, Inje University, Gimhae, Gyeongnam, 50834, Republic of Korea, Tel +1 82 55 320 3459, Fax +1 82 55 320 3940, Email minkahh@inje.ac.kr

Introduction: Extensive research has focused on identifying effective treatments for NAFLD, with numerous bioactive peptide candidates showing significant promise. In this research, a long-acting esculentin-2CHa(1-30)-coated AuNPs (ESC-ABD-AuNPs) was developed and the applicability was evaluated for their use in the treatment of non-alcoholic fatty liver disease (NAFLD).

Methods: ESC-ABD-AuNPs were synthesized by adopting a 1-step reduction process and the successful preparation of the nanoparticles (NPs) was assessed by various physical characterizations including transmission electron microscopy (TEM), ultraviolet-visible (UV-VIS) absorption spectra, dynamic light scattering (DLS), and Fourier Transform Infrared Spectroscopy (FT-IR). After the ESC-ABD-AuNPs were prepared, cytotoxicity, pharmacokinetics (PK), and biodistribution profiles were identified. Then, with a high-fat diet (HFD)-fed obese mice model, efficacy studies were carried out focused on their effects for anti-hyperglycemia and anti-NAFLD. Furthermore, the feasibility of loading a small molecule onto the NPs was evaluated for potential combination therapy.

Results: ESC-ABD-AuNPs were synthesized with an average hydrodynamic size of 120 (±10) nm and demonstrated good stability and an extended plasma half-life of 28.3 h. The NPs exhibited high liver accumulation and were well tolerated in cell viability tests. In PK and biodistribution studies, ESC-ABD-AuNPs showed prolonged retention in major organs, such as the pancreas and the liver. Therapeutic efficacy was demonstrated in the HFD-fed obese mice, where the ESC-ABD-AuNPs significantly reduced blood glucose levels, improved glucose tolerance, and mitigated liver fat accumulation. The ESC-ABD-AuNPs platform also showed potential for combination therapies, demonstrated by its ability to load obeticholic acid (OCA), a farnesoid X receptor (FXR) agonist, found effective for the treatment of NAFLD in clinical studies.

Conclusion: Overall, this study has demonstrated the promising potential of ESC-ABD-AuNPs as a novel treatment for NAFLD. This research suggests that ESC-ABD-AuNPs could be a significant advancement in drug delivery and liver disease treatment, particularly for combination therapies.

Keywords: non-alcoholic fatty liver disease, drug delivery, gold nanoparticles, obeticholic acid, esculentin-2CHa

Introduction

NAFLD is a prevalent liver condition, affecting over 25% of the global population.[1] It encompasses a spectrum of disorders, including nonalcoholic fatty liver (NAFL), nonalcoholic steatohepatitis (NASH), and cirrhosis. NAFL occurs when abnormal fat accumulation in liver cells leads to disease progression, advancing to NASH, which is marked by

Received: 24 September 2024
Accepted: 19 February 2025
Published: 17 March 2025

Graphical Abstract

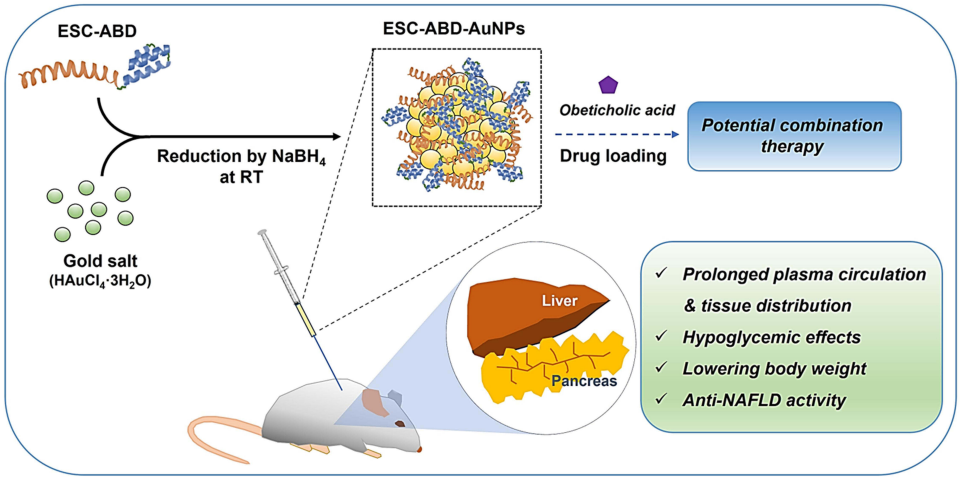

hepatocyte ballooning and inflammation.[2,3] Without intervention, NASH can further progress to cirrhosis, a severe and irreversible stage of liver damage.[4] Although a large portion of administered NPs are destined for the liver, they are often cleared, typically being phagocytosed by Kupffer cells.[5,6] Furthermore, the pathological change in the liver, specifically, in the late stage of NAFLD poses a significant challenge for hepatic drug delivery.

The AuNPs are receiving extensive interest in biomedical applications due to their ease of synthesis, excellent stability, biocompatibility, low toxicity, and distinctive optical properties.[7] The AuNPs are also highly effective carriers for delivering therapeutics. Their surface exhibits a strong affinity for amine and thiol functional groups, enabling biofunctionalization with protein therapeutics, peptides, and antibodies.[8] Furthermore, AuNPs have been reported to show no apparent toxicity to normal hepatocytes.[9,10]

Esculentin-2CHa(1–30) ("ESC") is a 30-mer peptide with deletion of 7 amino acids from the C-terminal of the original esculentin-2CHa derived from the skin secretion of the Chiricahua leopard frog (*Lithobates chiricahuensis*).[11–13] Previous reports have shown that the ESC possesses insulinotropic activity and can modulate glucose levels and reverse obesity in HFD-fed mice.[14,15] However, achieving the desired therapeutic effects required twice-daily administration for up to 28 days, suggesting its short plasma half-life.[15–17] In our previous study, we engineered a long-acting version of the ESC by genetic fusion to an albumin-binding domain (ABD).[18] This fusion protein ("ESC-ABD"), which includes a tandem repeat of three ESC units (3×ESC), an ABD, and "SUMO" as the expression partner, demonstrated an extended plasma half-life of 12 h following intravenous (i.v). administration.

In this study, a novel formulation called ESC-ABD-AuNPs, consisting of ESC-ABD-coated gold NPs, was developed and evaluated for its applicability in treating NAFLD. After successfully synthesizing ESC-ABD-AuNPs, its physico-chemical properties were characterized using dynamic light scattering (DLS), UV-VIS spectroscopy, and transmission electron microscopy (TEM). The formulation's hypoglycemic effects and efficacy in managing NAFLD were then evaluated in HFD-fed mice. This study further proposed the ESC-ABD-AuNPs could also serve as a potential carrier for delivering small molecule therapeutic agents to treat NAFLD.

Methods

The Preparation of Esculentin-2CHa-Albumin Binding Domain Fusion Protein Using Recombinant DNA Technology

The ESC-ABD was prepared following the protocol by Lee et al.[18] A colony of pET28a-SUMO-3×ESC-ABD plasmid transformed BL21 competent *E. coli* cells were added to 50 mL of LB medium including 80 mg/mL kanamycin. The

culture was incubated overnight at 37°C with 250 rpm shaking. The overnight culture was then transferred to 1 L of LB medium (80 mg/mL kanamycin; Fisher Scientific, Pittsburgh, USA) and then incubated at identical conditions until the OD_{600} reached 0.9–1.0. At this point, 0.5 mm Isopropyl-b-thiogalactopyranoside (IPTG; Fisher Scientific, Pittsburgh, USA) was added, and then the culture was further incubated for 4 h. After the cells were harvested by centrifugation, the pellets were resuspended in 20 mm PBS (containing 300 mm NaCl; pH 7.4). The cells were lysed by sonication and centrifuged at 8000 rpm for 10 min. The supernatant was collected and purified using Talon affinity resins. The acquired ESC-ABD was further purified using an ultra-centrifugal filter unit (MWCO: 30 kDa). Protein purity and integrity were assessed with SDS-PAGE on a 10% gel, and the final protein concentration was determined by the BCA assay. The purified protein was stored at 4°C for future use.

The Chemical Synthesis of Esculentin-2CHa-Albumin Binding Domain-Coated Au Nanoparticles

The scheme of the particle synthesis procedures are illustrated in Figure 1. Three milligrams of ESC-ABD (dissolved in 1 mL of PBS) were added to a glass vial, followed by the addition of 1 mg of $NaBH_4$ (the reducing agent; dissolved in 1 mL of DDW) and 100 µL of 30 mg/mL $HAuCl_4{\cdot}3H_2O$ (equivalent to 1.5 mg Au; Sigma Aldrich, St. Louis., MO, USA). The reaction mixture was incubated at room temperature (RT) with stirring at 1000 rpm for 20 min. The NPs were purified using an ultra-centrifugal filter unit (MWCO: 100 kDa) to remove unreacted protein and $HAuCl_4{\cdot}3H_2O$. The final sample volume was adjusted to 1 mL and stored at 4°C for future use. The Bradford assay was used to determine the protein concentration.

The Electron Microscopy

The size, morphology, and composition of ESC-ABD-AuNPs were analyzed using Bio transmission electron microscopy (BIO-TEM, 120 kV) and high-resolution field emission TEM (HR-TEM, 300 kV) equipped with energy dispersive spectroscopy (EDS). The UV-VIS absorption spectra of the samples were acquired using a BioTek Synergy H1 hybrid Multi-Mode Reader (Winooski, VT, USA). DLS (Zetasizer Nano ZS, Malvern Panalytical Ltd., Malvern, UK) was employed to measure the hydrodynamic size and zeta potential of the NPs. The size stability of the ESC-ABD-AuNPs, at 4°C storage condition, was evaluated over 5 consecutive days by monitoring the particle appearance and size. Lastly, the FT-IR was conducted with an FT-IR micro-spectrometer (VERTEX 80v, Bruker, Billerica, MA, USA).

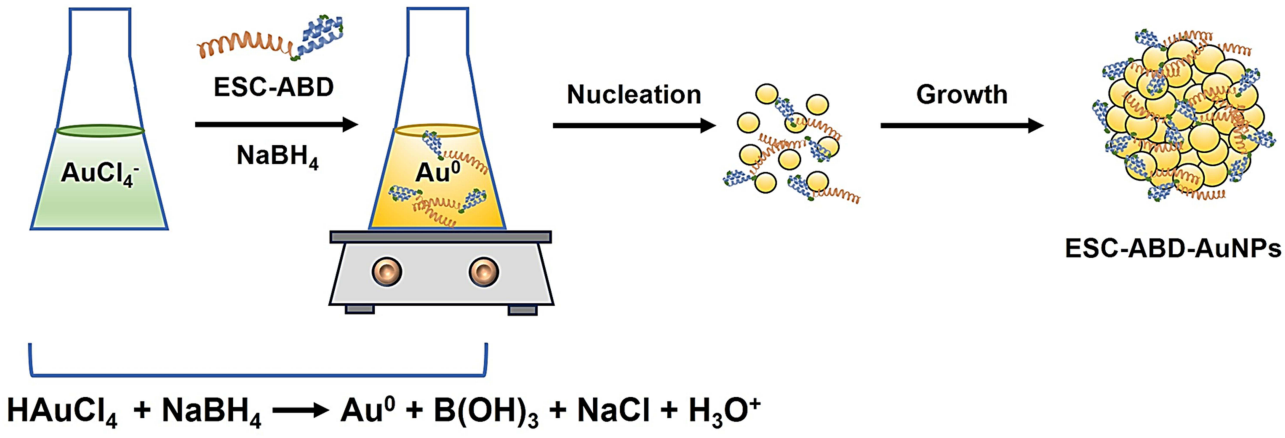

Figure 1 Scheme of the synthesis of ESC-ABD-AuNPs. (ESC-ABD-AuNPs: ESC-ABD-coated gold nanoparticles).

https://doi.org/10.2147/IJN.S497645

Evaluation of the Loading Efficiency of Obeticholic Acid to the Esculentin-2CHa-Albumin Binding Domain-Coated Au Nanoparticles

The feasibility of loading small molecule drugs to the ESC-ABD-AuNPs was assessed using obeticholic acid (OCA) as the model drug. The OCA-loaded ESC-ABD-AuNPs (ESC-ABD-AnNP/OCA) were prepared by adding different feed amounts of OCA (2 mg, 4 mg, and 6 mg) to the mixture of ESC-ABD/$NaBH_4$/Au during the synthesis of the ESC-ABD-AuNPs. The unloaded OCA was purified from the ESC-ABD-AuNPs/OCA using an ultra-centrifugal filter unit (MWCO: 100 kDa; 3 cycles for 10 min each). After purification, the amount of OCA loaded onto the NPs was quantified using the Total Bile Acid (TBA) Colorimetric Assay Kit (Elabscience, Wuhan, China). The OCA loading efficiency (%) was determined by dividing the amount of OCA in the final loaded sample by the fed OCA and multiplying 100.

Determination of Cell Viability Against Esculentin-2CHa-Albumin Binding Domain-Coated Au Nanoparticles

The cell viability was determined using 3 relevant cell lines: murine melanoma B16F10 cells, the murine pancreatic β-cell line MIN6, and human hepatocellular carcinoma HepG2 cells. The B16F10 and HepG2 cells were purchased from ATCC (Manassas, VA, USA). MIN6 cells were kindly given by Dr. Min Gap Kim (Gyeongsang National University, Jinju, Republic of Korea).[19,20] The selection of the cell lines was based on the organs which are important for the in vivo behavior of the particles. The B16F10 represents the absorption site (skin), while the MIN6 and HepG2 stand for the primary action sites (pancreas and liver). The liver is also the main elimination site. The cells were cultured in Dulbecco's Modified Eagle Medium (DMEM, Gibco, Grand Island, USA) supplemented with 10% fetal bovine serum (FBS), 1% penicillin-streptomycin, and 1% antibiotic-antimycotic. The cells were maintained in an incubator at 37°C with 5% CO_2. For the study, the cells were separately seeded onto 96 wells (B16F10: 5×10^3 cells per well, MIN6 and HepG2: 1×10^4 cells per well). After 24 h, the cells were treated with various concentrations (0–150 μgAu/mL) of ESC-ABD-AuNPs, and further incubated for 48 h. The cell viability was determined using the WST-1 assay (iNtRON Biotechnology, Daejeon, Republic of Korea).

Animal Studies

All the animal studies were complied with the National Institute of Health Guidelines on the Use of Laboratory Animals, following the protocol approved by the GNU's Committee for Animal Research (GNU-230615-M0131).

Establishment of Animal Models

For pharmacokinetics (PK) and biodistribution studies, 6-week-old C57BL/6 mice (KOATECH, Pyeongtaek, Republic of Korea) were used. The mice were housed at Gyeongsang National University's animal facilities, where they had ad libitum access to food and water and were maintained on a 12 h light-dark cycle. The study was initiated after a week of acclimation to the new housing environment. For efficacy studies, 3-week-old C57BL/6 mice were used after inducing obesity by feeding an HFD of 60% kcal fat chow (5.24 kcal/g, Research Diets, New Brunswick, NJ, USA) for 12 weeks. The average body weight of the HFD-fed mice when the study was started was 45.2 g and the concentrations of ESC-ABD and ESC-ABD-AuNPs were set to inject an average of 150 and 300 μL volumes, respectively.

Evaluation of the Pharmacokinetic Profiles of Esculentin-2CHa-Albumin Binding Domain-Coated Au Nanoparticles

Prior to the study, to trace the ESC-ABD-AuNPs, the ESC-ABD of the NPs was labeled with a fluorescence dye (Rhodamine B isothiocyanate (RITC); Amresco Inc., Germany). Briefly, in a glass vial, 1 mL of ESC-ABD (5 mg/mL) was added, followed by the dropwise addition of 0.25 mg of RITC (dissolved in 100 μL of DMSO; 3-fold higher molar ratio to the protein). The reaction mixture was incubated at RT for 2 h, gently stirring in the dark. After incubation, the RITC-labeled ESC-ABD (RITC-ESC-ABD) was initially purified using Talon affinity resins, and then further purified with an ultra-centrifugal filter unit (MWCO: 10 kDa). The final sample volume was adjusted to 1 mL. After the RITC-ESC-ABD was prepared, the AuNP was synthesized by adopting the identical

protocol for the ESC-ABD-AuNPs. The final volume was again adjusted to 1 mL and stored at 4°C. Bradford protein assay was performed to determine the protein concentration, and fluorimetry was used to quantify the dye.

For the PK experiments, the C57BL/6 mice were administered with RITC-ESC-ABD-AuNPs (600 μg/mouse as ESC-ABD) via subcutaneous (s.c). injection. Blood samples were collected at 0, 0.5, 1, 2, 4, 8, 24, 48, and 72 h post-administration. The blood was centrifuged at 4000 rpm for 5 min to obtain plasma. Plasma samples were analyzed using a fluorometric method with the FOBI fluorescent in vivo imaging system (Cellgentek, Osong, Republic of Korea). PK profiles were determined by performing a non-compartmental analysis of the plasma concentration versus time data using the Phoenix WinNonlin® program (Certara LP., Princeton, NJ, USA).

Assessment of the Biodistribution Profiles of Esculentin-2CHa-Albumin Binding Domain-Coated Au Nanoparticles

RITC-ESC-ABD-AuNPs (600 μg/mouse as ESC-ABD) were administered to C57BL/6 mice via s.c. injection. On days 1, 3, 5, and 7 post-injections, the mice were euthanized, and major organs, such as the liver, spleen, kidney, pancreas, intestine, lung, heart, and brain, were collected. The FOBI system was used to capture both the fluorescent and brightfield images of the organs and create overlaid images. The integrated density was measured by identifying each organ's region of interest (ROI).

Glucose Tolerance Test of Esculentin-2CHa-Albumin Binding Domain-Coated Au Nanoparticles in High Fat-Diet Fed Obese Mice

The HFD-fed obese C57BL/6 mice were divided into 3 groups (N=10) including 1) Control, 2) ESC-ABD (50 nmol/kg), and 3) ESC-ABD-AuNPs (50 nmol/kg as ESC-ABD). After 16 h fasting, mice in each group received either saline, ESC-ABD, or ESC-ABD-AuNPs via s.c. injection. One h later, all mice were administered with D-glucose (2 g/kg body weight; Sigma-Aldrich), and blood glucose levels were measured at 0, 30-, 60-, 90-, and 120-min post-glucose administration using a Roche Accu-Chek glucometer (Mannheim, Germany).

Single Administration Efficacy Study for Esculentin-2CHa-Albumin Binding Domain-Coated Au Nanoparticles

Another group of HFD-fed obese C57BL/6 mice were divided into 3 groups (N=10). The mice received s.c. injection of either saline, ESC-ABD (50 nmol/kg), or ESC-ABD-AuNPs (50 nmol/kg as ESC-ABD). For 7 days after administration, blood glucose levels and body weights were monitored daily.

Long-Term (4-Week) Efficacy Study for Esculentin-2CHa-Albumin Binding Domain-Coated Au Nanoparticles

After dividing the HFD-fed C57BL/6 mice into 3 groups (N=10), each group was administered one of the following via s.c. injection: saline, ESC-ABD (50 nmol/kg), or ESC-ABD-AuNPs (50 nmol/kg as ESC-ABD). The treatments were given twice weekly for 4 weeks, and blood glucose levels and body weights were monitored. At the end of the study, a GTT was conducted.

After the 4-week efficacy study was terminated, the mice were fasted overnight and anesthetized with a mixture of ketamine/xylazine (87.5/12.5 mg/kg). The blood samples were then collected from the left ventricle of the hearts and serum samples were sent to the Southeast Medi-Chem Institute (Pusan, Republic of Korea) for analyses of fasting serum glucose, AST, ALT, triglyceride (TG), and total cholesterol (TC). In addition, after euthanization of the mice, the liver and pancreas were harvested, fixed in 4% paraformaldehyde for 12 h at 4°C, and then embedded in paraffin. After embedding, the tissues were sliced into sections with 5 μm thickness. The tissue sections were deparaffinized and stained with the reagents of hematoxylin and eosin (H&E, Sigma-Aldrich). A part of liver tissues were frozen and the sliced liver sections were stained with Nile Red (Sigma Aldrich). All the images of the tissue sections were taken by a BX51 light microscope (Olympus, Tokyo, Japan). The Nile Red-stained area (250 × 250 μm^2; percent of total area) was calculated from the images (N = 5) with i-Solution (IMT i-Solution Inc., Vancouver, BC, Canada). For the pancreatic section, the percentage of pancreatic islet area was determined using i-Solution software (IMT i-Solution Inc., Vancouver, BC, Canada).

Cellular Evaluation of the Insulin Secretion by Esculentin-2CHa-Albumin Binding Domain-Coated Au Nanoparticles

The MIN6 cells (200,000 cells per well) were seeded onto 24 well-plates and incubated in a DMEM medium (including 10% fetal bovine serum albumin) for 48 h. After that, the cells were washed with Krebs-Ringer bicarbonate (KRB) buffer (composed of 115 mm NaCl, 4.7 mm KCl, 1.28 mm $CaCl_2$, 1.2 mm KH_2PO_4, 1.2 mm $MgSO_4$, and 10 mm $NaHCO_3$) including 0.1% BSA. Then, the cells were incubated with 0.1 or 1 μM of either ESC-ABD or ESC-ABD-AuNPs in KRB buffer (with 0.1% BSA and 5 mm glucose) for 2 h. KRB buffers with 5 mm glucose and 25 mm glucose were used as negative control and positive control, respectively. After incubation, the secreted insulin content was quantified by ELISA (mouse insulin ELISA kit, Shibayagi Co. Ltd., Gunma, Japan).

Statistical Analysis

The data were expressed as the mean (± SEM; standard error of the mean). Statistical differences among groups were assessed using 1-way ANOVA test. Tukey's multiple comparison tests were employed as the post hoc analysis (Prism version 10.0, GraphPad). Results were considered statistically significant if $p < 0.05$.

Results

The Chemical Synthesis and Physical Characterization of Esculentin-2CHa-Albumin Binding Domain-Coated Au Nanoparticles

In our study, we synthesized ESC-ABD-AuNPs using a chemical reduction method with $NaBH_4$ as the reducing agent. The addition of $NaBH_4$ caused a color change from colorless to reddish-brown; suggesting the successful synthesis of the NPs (Figure 2A). According to the BIO-TEM images, the ESC-ABD-AuNPs appeared to possess irregular shapes (Figure 2B), while the HR-TEM images showed conglomerates of generally spherical units (Figure 2C). In the scanning transmission electron microscopic (STEM) image of the NPs, the distribution profiles of carbon (C) and nitrogen (N)

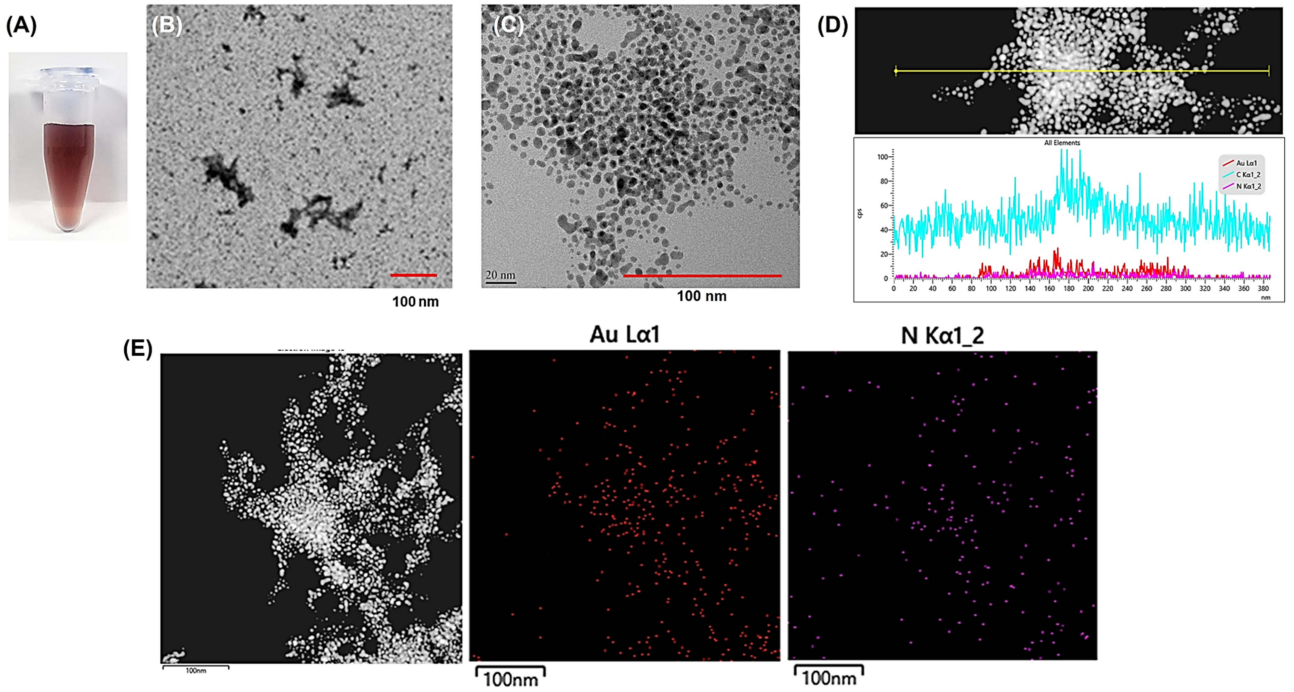

Figure 2 Electron microscopy of ESC-ABD-AuNPs. (**A**) Representative image of ESC-ABD-AuNPs. (**B**) BIO-transmission electron microscopic (BIO-TEM) and (**C**) high-resolution TEM (HR-TEM) images of ESC-ABD-AuNPs. (**D**) Scanning transmission electron microscopic (STEM) image of the particles and elemental distribution of carbon (C), nitrogen (N), and gold (Au). (**E**) STEM image of the particles and 2D distribution of the Au and N.
Abbreviation: ESC-ABD-AuNPs, ESC-ABD-coated gold nanoparticles.

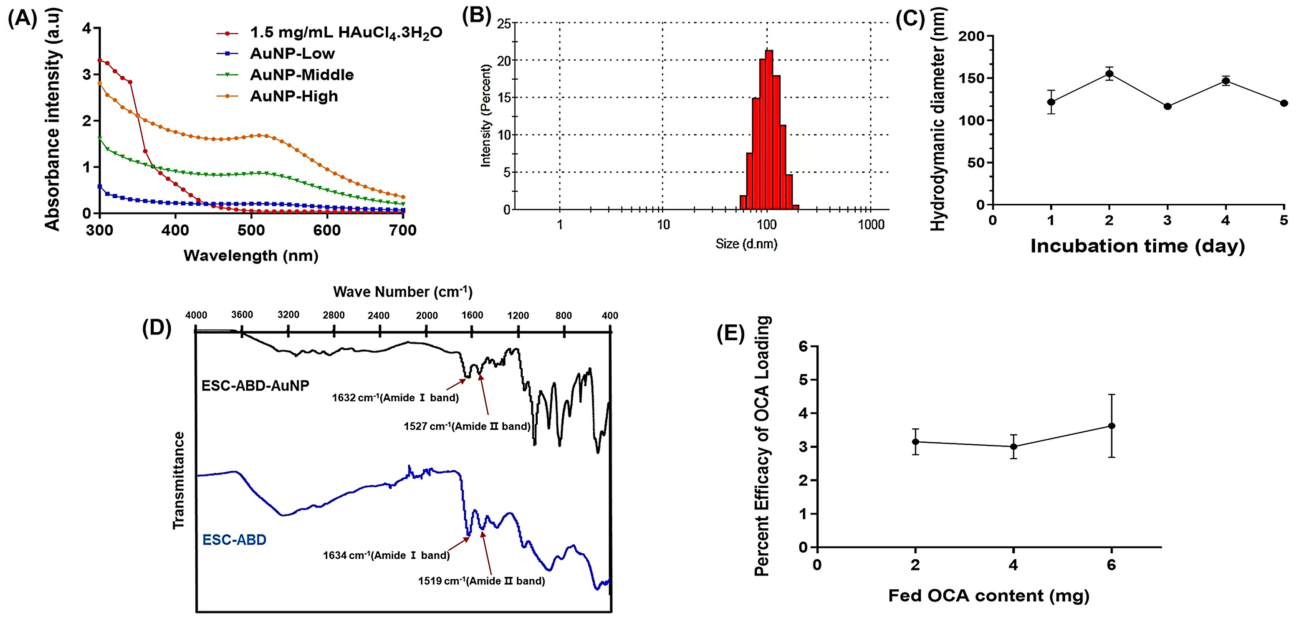

Figure 3 Physical characterization of ESC-ABD-AuNPs. (**A**)The UV-VIS spectrometric analysis of ESC-ABD-AuNPs. (**B**) Hydrodynamic size distribution and (**C**) size stability of ESC-ABD-AuNPs. (**D**) Fourier transform infrared (FT-IR) spectrum of ESC-ABD-AuNPs. (**E**) Loading study results of obeticholic acid (OCA) loading onto ESC-ABD-AuNPs.

which represents the protein, and gold (Au) were generally overlapping at the region of the NPs (Figure 2D). Also, when compared the 2D distribution of Au and N, they were generally overlapping. (Figure 2E). The UV-visible spectra of ESC-ABD-AuNPs (Figure 3A) displayed a prominent peak, in contrast with the Au ion, between 500–600 nm, consistent with the previous report by Haiss et al.[21] DLS analysis revealed an average NP size of 120 (±10) nm with a PDI of 0.16 (Figure 3B). The particles demonstrated good stability, with no visible aggregation observed over 5 days at storage conditions (Figure 3C). Finally, according to the FT-IR spectra, as shown in Figure 3D, the characteristic peaks of ESC-ABD protein (bands for amide I and II: 1634 and 1519 cm^{-1}, respectively) were found from the spectrum of ESC-ABD-AuNPs (at 1632 and 1527 cm^{-1}, respectively). Overall, the successful synthesis of the ESC-ABD-AuNPs was evidenced by all the physical characterization.

Obeticholic Acid Loading Efficiency to Esculentin-2CHa-Albumin Binding Domain-Coated Au Nanoparticles

As shown in Figure 3E, the loading efficiency of OCA onto ESC-ABD-AuNPs ranged similarly from 3.0–3.6% with OCA feed amounts of 2–6 mg. These results indicated that the ESC-ABD-AuNPs could indeed serve as a carrier for delivering small-molecule drugs (like OCA).

Cytotoxicity of Esculentin-2CHa-Albumin Binding Domain-Coated Au Nanoparticles

In the cellular toxicity studies, conducted using B16F10, MIN6, and HepG2 cell lines, the ESC-ABD-AuNPs exhibited no significant toxicity, with over 80% cell viability (Figure 4). Even at the highest concentration of 150 μgAu/mL, the treated cells showed no adverse effects, indicating the "safeness" of the NPs. This low cytotoxicity supports the feasibility of using these NPs for chronic therapies without toxicity concerns.

Pharmacokinetic Profile Analyses of Esculentin-2CHa-Albumin Binding Domain-Coated Au Nanoparticles

The plasma concentration-versus-time profiles of ESC-ABD-AuNPs are presented in Figure 5A, with key pharmacokinetic parameters summarized in Table 1. Following s.c. administration, the average plasma half-life of ESC-ABD-AuNPs was

https://doi.org/10.2147/IJN.S497645

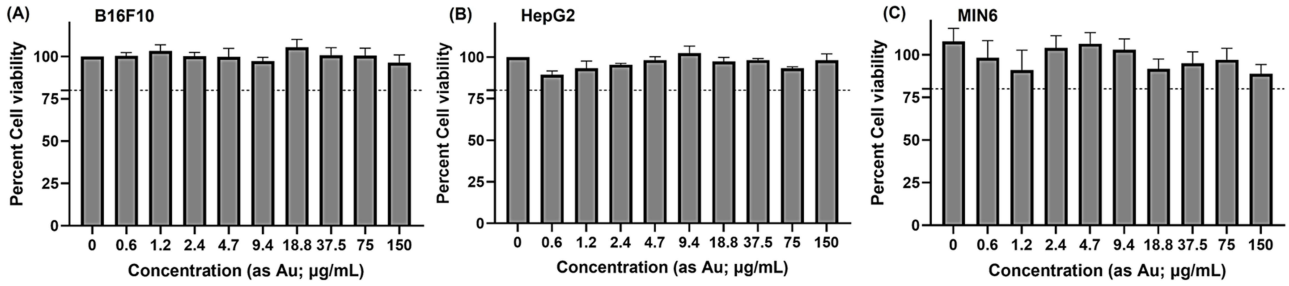

Figure 4 Cytotoxicity profile of ESC-ABD-AuNPs. (**A**) B16F10, (**B**) HepG2, and (**C**) MIN6 cells were tested for the cytotoxicity assays.
Abbreviation: ESC-ABD-AuNPs, ESC-ABD-coated gold nanoparticles.

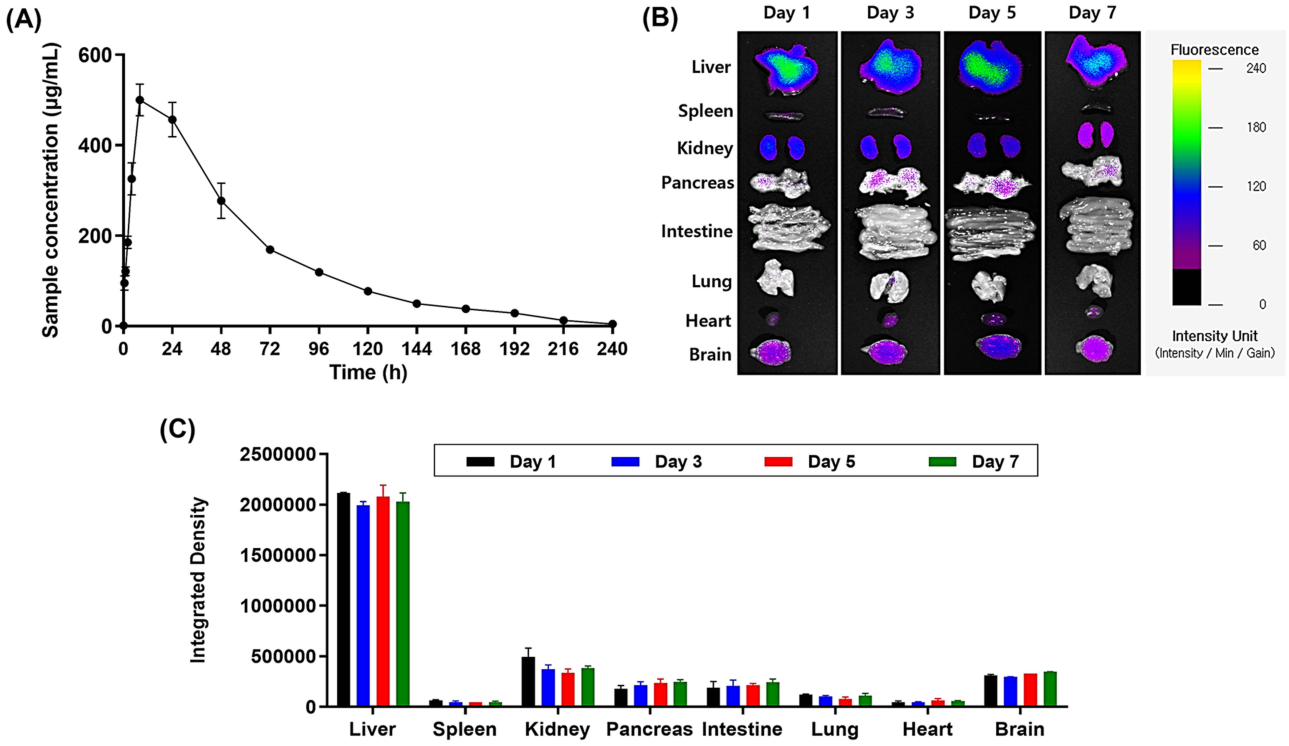

Figure 5 PK and biodistribution profiles of ESC-ABD-AuNPs. (**A**) Average plasma concentrations-versus-time profiles of ESC-ABD-AuNPs after s.c. injection in C57BL/6 mice (N=3). (**B**) Representative images of the major organs of mice after administration of RITC-labeled-ESC-ABD-AuNPs. (**C**) Fluorescent intensity profiles RITC-labeled-ESC-ABD-AuNPs in major organs along different time points.
Abbreviations RITC, rhodamine B isothiocyanate; ESC-ABD-AuNPs, ESC-ABD-coated gold nanoparticles.

determined to be 28.3 h, indicating a relatively prolonged duration in the plasma. This value is comparable to the ESC-ABD alone (plasma half-life: 23.5 h by s.c. injection), reflecting the stability and long-acting nature of the ESC-ABD-AuNPs. This long plasma half-life makes it potentially advantageous for reducing dosing frequency in therapeutic applications, particularly for treating chronic conditions like NAFLD where consistent therapeutic levels of the drug are required over extended

Table 1 PK Profiles of ESC-ABD-AuNPs

Samples	C_{max} (µg/mL)	T_{max} (h)	$AUC_{0-\infty}$ (h µg/mL)	$T_{1/2}$ (h)	MRT (h)
ESC-ABD-AuNPs (s.c.)	500 (± 70.74)[a]	8 (± 0)	34,247 (± 4130)	28.27 (± 9.854)	53.19 (± 4.959)

Note: [a]Standard error values of mean were exhibited in the parenthesis.
Abbreviations: ESC-ABD-AuNPs, ESC-ABD-coated gold nanoparticles; Cmax, maximum concentration; Tmax, timepoint at which reached maximum concentration; AUC, area under the curve; $T_{1/2}$, plasma half-life; MRT, mean residence time.

periods to ensure effective disease management. This extended duration in circulation may also enhance the overall efficacy of the treatment while minimizing the need for frequent administration, thereby improving patient compliance.

Biodistribution Profiles of Esculentin-2CHa-Albumin Binding Domain-Coated Au Nanoparticles

The biodistribution profile of ESC-ABD-AuNPs (Figure 5B and C) revealed sustained detectability in most major organs for up to 7 days following administration, highlighting the NPs' ability to remain in the body over an extended period. Notably, a substantial accumulation of the ESC-ABD-AuNPs was observed in the liver. This prolonged and selective retention in the liver suggests that ESC-ABD-AuNPs may serve as an effective drug for NAFLD treatment.

Single Administration Efficacy Study for Esculentin-2CHa-Albumin Binding Domain-Coated Au Nanoparticles

The single-treatment study with ESC-ABD-AuNPs showed that its hypoglycemic effects were comparable to those observed with ESC-ABD (Figure 6A), indicating that both treatments effectively lowered blood glucose levels to a similar degree. This suggests that ESC-ABD-AuNPs retain the essential glucose-regulating properties of ESC-ABD, making it a promising candidate for managing hyperglycemia. However, ESC-ABD demonstrated superior efficacy in body weight management (Figure 6B).

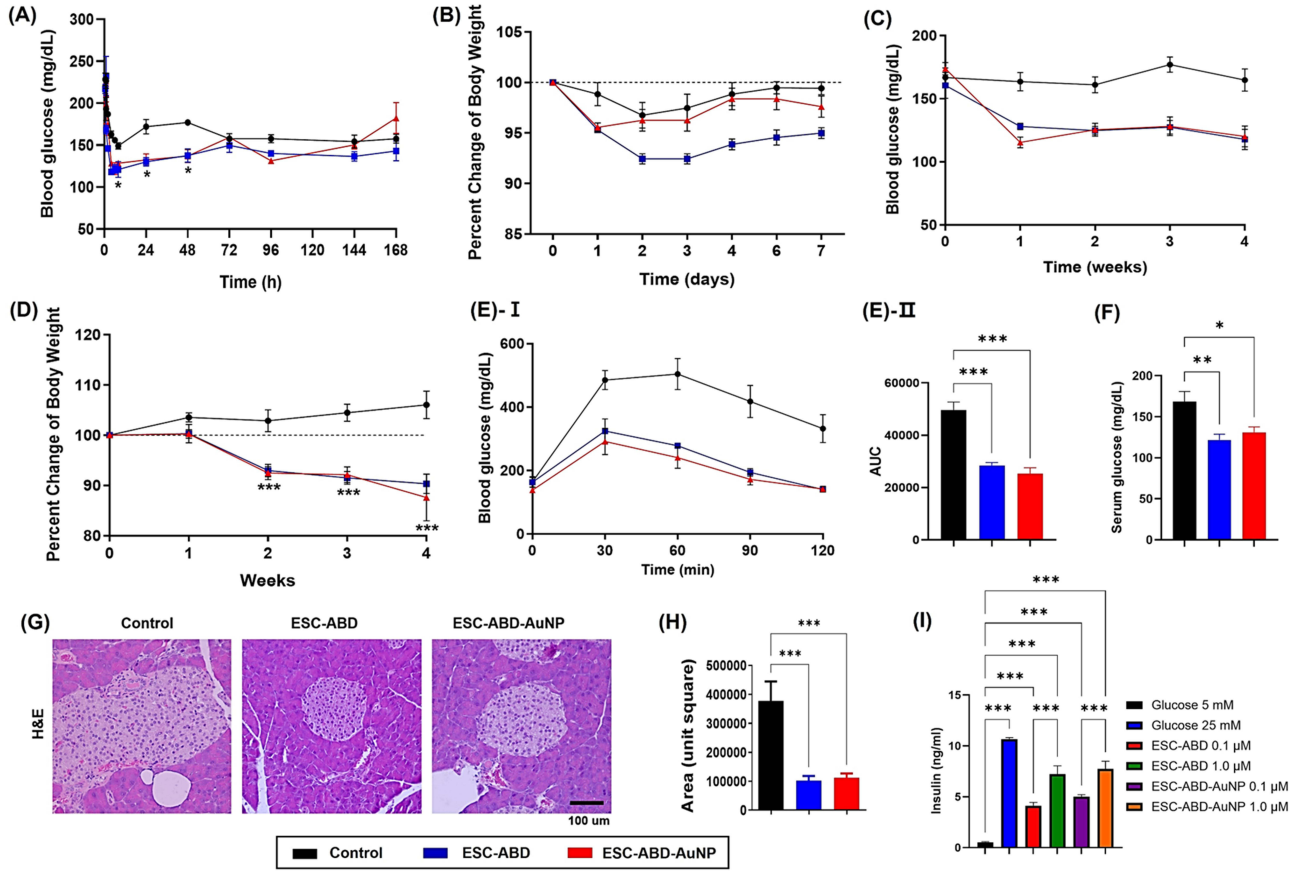

Figure 6 Hypoglycemic effects of ESC-ABD-AuNPs in HFD-fed C57BL/6 mice. (**A**) The mice's blood glucose level and (**B**) body weight change during the single administration efficacy study. (**C**) Blood glucose levels, and (**D**) change in body weight of the mice during the long-term (4-week) efficacy study. After 4 weeks of treatment, (**E**) glucose tolerance test (GTT) was carried out (**I**: Blood glucose levels, **II**: AUC [area under curves "**I**"] values), and (**F**) fasting serum glucose levels were measured. (**G**) Representative pancreas sections stained with H&E staining. (**H**) Pancreatic islet size comparison. (**I**) Glucose-dependent insulin release from MIN6 cells by ESC-ABD-AuNPs. The statistically significant differences among the groups were compared by one-way ANOVA (Tukey's multiple comparison test as the post hoc test). *P < 0.05, **P < 0.01, ***P < 0.001.
Abbreviations: ESC-ABD-AuNPs, ESC-ABD-coated gold nanoparticles; HFD, high-fat diet.

https://doi.org/10.2147/IJN.S497645

Therapeutic Effects of 4-Week Treatment of Esculentin-2CHa-Albumin Binding Domain-Coated Au Nanoparticles

Hypoglycemic Effects

Throughout the 4-week treatment with ESC-ABD-AuNPs, blood glucose levels remained consistently low, demonstrating sustained glycemic control over the entire study period (Figure 6C). In addition to glucose regulation, a significant reduction in body weight was observed (Figure 6D), further highlighting the positive metabolic effects of the treatment. Importantly, the ESC-ABD-AuNPs formulation was well tolerated by the mice, with no signs of toxicity or adverse effects throughout the treatment duration, indicating its safety profile for extended use. GTT was conducted at the end of the 4 weeks (Figure 6E). The results showed that ESC-ABD-AuNPs significantly improved glucose tolerance equivalent to ESC-ABD. Consistently, the fasting serum glucose levels were significantly reduced (Figure 6F). This indicates that ESC-ABD maintained its therapeutic properties when incorporated into the AuNP platform, suggesting that the nanoformulation did not compromise the efficacy of the ESC-ABD. These findings not only demonstrate that ESC-ABD-AuNPs are an effective platform for glucose regulation and weight management but also open the door for further applications in combination therapies. By using ESC-ABD-AuNPs as a delivery system, it may be possible to incorporate additional therapeutic agents, enhancing the treatment outcomes for NAFLD and its related complications. The potential for additive or synergistic effects when combining therapies with ESC-ABD-AuNPs may provide more comprehensive metabolic control, addressing multiple pathways involved in NAFLD progression.

Effects on the Pancreatic Islets

In Figure 6G, the pancreatic islets of the control group exhibit abnormal enlargement, reflecting an adaptive response of β-cells to heightened insulin demand. This enlargement is indicative of both hypertrophy (enlargement of individual β-cells) and hyperplasia (an increase in the number of β-cells), mechanisms that temporarily compensate for insulin resistance. While this response may initially help maintain glucose homeostasis, prolonged stress on β-cells can lead to dysfunction and eventual damage, contributing to the progression of metabolic disorders such as type 2 diabetes. As shown in Figure 6H, treatment with ESC-ABD successfully restored the pancreatic islet size to normal levels, suggesting an improvement in β-cell health and function. This normalization of islet size indicates that ESC-ABD helps alleviate the stress on β-cells, potentially by reducing the insulin demand, thereby preventing the maladaptive hypertrophy responses. To verify the mechanism of the hypoglycemic effects, when the ESC-ABD-AuNPs were added to MIN6 cells in the presence of 5 mm glucose, significant insulin secretion was observed, equivalent to the ESC-ABD (Figure 6I). These results suggested that the ESC-ABD-AuNPs could improve hyperglycemia by exerting direct insulinotropic effects.

Inhibition of Hepatic Fat Accumulation

As shown in Figure 7A and B, the ESC-ABD-AuNPs-treated group exhibited marked improvements in liver color and size, indicating a reversal of NAFLD-related liver enlargement and discoloration. These visual improvements suggest that ESC-ABD-AuNPs effectively mitigated liver damage commonly associated with NAFLD. Liver tissue sections were prepared and analyzed to evaluate the therapeutic effects of ESC-ABD-AuNPs on NAFLD. Further analysis of the H&E-stained sections (Figure 7C) and the Nile red-stained sections (Figure 7D and E) revealed a significant reduction in lipid accumulation within hepatocytes in both the ESC-ABD and ESC-ABD-AuNPs-treated groups. This reduction in intracellular lipid droplets indicates that the treatment effectively reduced fat buildup in the liver, a hallmark of NAFLD, suggesting improved lipid metabolism and decreased steatosis.

In addition to histological improvements, biochemical markers of liver function were assessed. AST (Figure 7F) and ALT (Figure 7G), both key indicators of liver injury, were significantly reduced in the ESC-ABD-AuNPs-treated group compared to the control. These reductions imply that the treatment prevented liver damage and promoted the restoration of normal liver function. The TG level did not significantly change, but the TC levels were considerably reduced by the treatment of ESC-ABD-AuNPs (Figure 7H and I). The combination of histological and biochemical data demonstrated that ESC-ABD-AuNPs possessed a substantial therapeutic efficacy on NAFLD.

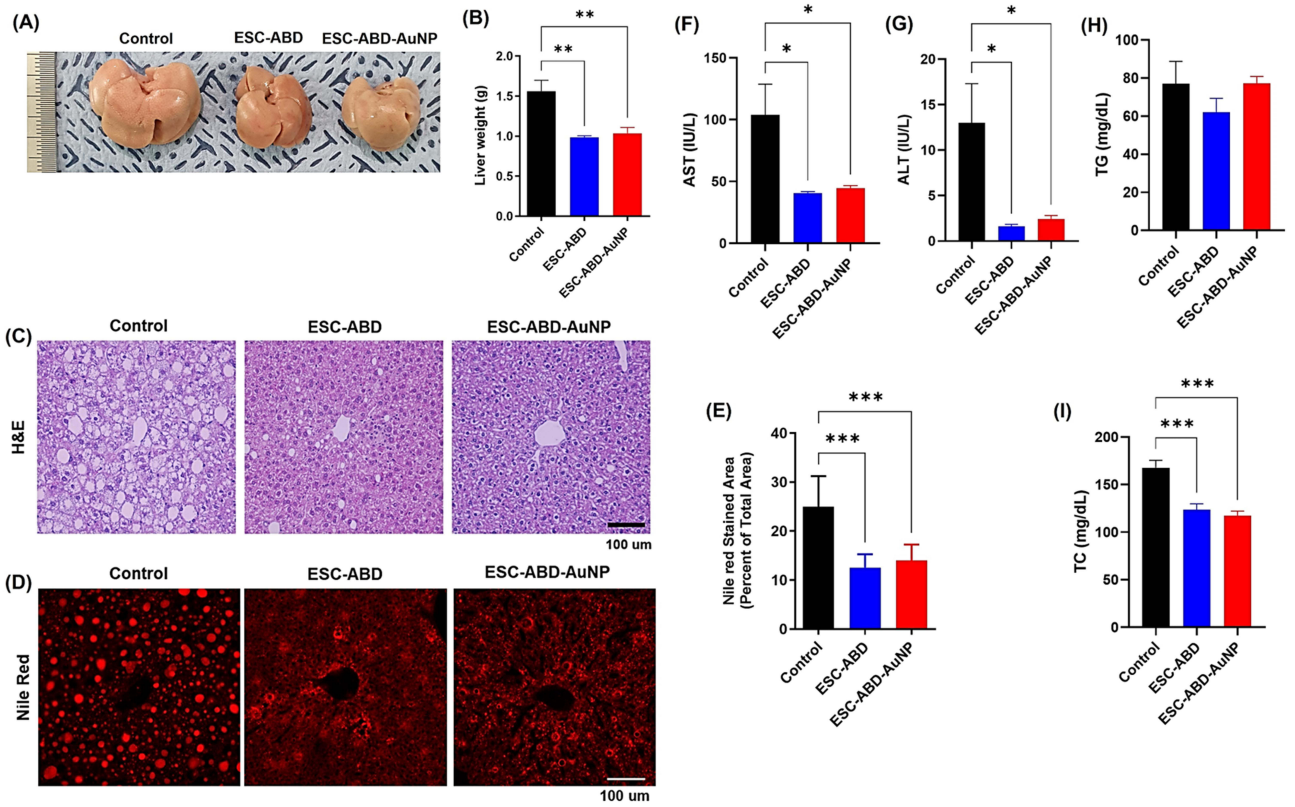

Figure 7 Therapeutic effects of ESC-ABD-AuNPs on NAFLD in the HFD-fed C57BL/6 mice. (**A**) Representative images of the livers harvested after the long-term (4 weeks) treatment. (**B**) Average liver weights. (**C**) Representative images of the liver sections stained with H&E staining. (**D**) Representative images of the liver sections stained with Nile Red. (**E**) Nile Red stained area (percent of total area) (N=5). Hematological analysis results (**F**) aspartate aminotransferase (AST), (**G**) alanine aminotransferase (ALT), (**H**) triglyceride (TG), and (**I**) total cholesterol (TC). The statistically significant differences among the groups were compared by one-way ANOVA (Tukey's multiple comparison test as the post hoc test). *P < 0.05, **P < 0.01, ***P < 0.001.

Abbreviations: ESC-ABD-AuNPs, ESC-ABD-coated gold nanoparticles; HFD, high-fat diet.

Discussion

Nanotechnology has garnered considerable attention in the biomedical field due to its wide-ranging applications in diagnostics, drug delivery, imaging, and beyond.[22–24] The NPs are highly adaptable, making them ideal carriers for various therapeutic agents, including proteins, peptides, small molecules, and nucleic acids (DNA and RNA).[25] Among the NPs, AuNPs have gained great popularity, in part, due to the simplicity in their synthesis.[26–28] The chemical reduction method is the most widely used approach. In this method, reducing agents convert gold ions (Au^{3+}) into gold atoms (Au^{0}), leading to the formation of NPs.[29] Notably, by adjusting the reaction conditions, the size of AuNPs could be precisely controlled which could be crucial to the success of their use for NAFLD treatment.

Extensive research has focused on identifying effective treatments for NAFLD, with numerous bioactive peptide candidates showing significant promise. Ojo et al were the first to report that the peptide ESC possesses substantial anti-diabetic and insulinotropic properties, promoting insulin secretion and improving glucose tolerance in HFD-fed mice.[15] The cationic nature of ESC enhances its interaction with the β-cell membrane, directly influencing insulin release.[16] Studies have indicated that administering ESC to HFD-fed mice improved their blood glucose profiles, reduced insulin resistance, and helped decrease body weight.[17] Given the direct connection between obesity, diabetes, and NAFLD, ESC's potential to address these critical issues presents a promising avenue for its use in alleviating NAFLD.[17] However, therapeutic peptides often face challenges due to their rapid degradation in the body. In our previous study, we introduced a fusion protein SUMO-3×ESC-ABD, which combines ESC and ABD to extend its plasma half-life.[18] This protein, having a prolonged half-life of 12.1 h, demonstrated that it could effectively regulate blood glucose and body weight and reduce liver fat in HFD-fed mice, highlighting its potential in the treatment of NAFLD.[18]

https://doi.org/10.2147/IJN.S497645

In this study, ESC-ABD-AuNPs were developed to overcome the challenge of targeted drug delivery to the liver for NAFLD treatment. The NPs were successfully synthesized, displaying a reddish-brown color (Figure 2A), with an average size of 120 (±10) nm and a PDI of 0.16 (Figure 3B). They demonstrated good stability at 4°C for up to 5 days without any signs of aggregation (Figure 3C). Among various factors that could affect the fate of the NPs that reach the liver, the size of the NPs plays a critical role in their delivery to hepatocytes.[30–32] The liver sinusoidal endothelial cells (LSECs), with fenestrae that allow the passage of particles smaller than 200 nm, illustrate the importance of size in biodistribution.[33,34] According to an interesting study by Park et al about the hepatic distribution of nanoparticles, PLGA NPs with an average size of 271 nm were mostly found in non-parenchymal cells, including 15% in Kupffer cells (KCs), 20% in LSECs, 1% in hepatic stellate cells (HSCs), and only 4% in hepatocytes.[35,36] Overall, this study's results implied that effective NAFLD treatment by NPs heavily relied on controlling their sizes under 200 nm. In this line, the size of ESC-ABD-AuNPs could be considered sufficient for hepatic delivery.

The safety profile of ESC-ABD-AuNPs was evaluated using various and significant cell lines (B16F10, HepG2, and MIN6 cells) (Figure 4). In all 3 cell lines tested, the ESC-ABD-AuNPs were well tolerated, with cell viability remaining above 80%, even at the highest concentration of 150 μgAu/mL.

Next, PK and biodistribution studies were conducted to evaluate the plasma residence time of the ESC-ABD-AuNPs. The PK profile revealed an extended half-life of 28.3 h (Figure 5A). The time to reach maximum plasma concentration (T_{max}) was 8 h, indicating a delay in the absorption from the s.c. injection site into the systemic circulation. However, considering the similarity of the plasma half-life to the ESC-ABD (23.5 h), the prolonged plasma half-life (28.3 h) appears more likely attributed to the successful binding of ESC-ABD-AuNPs to the plasma albumin, enabling the FcRn-mediated recycling. Consistent with the PK study results, the biodistribution profiles also showed extended retention of ESC-ABD-AuNPs in major organs, particularly the liver, for up to 7 days (Figure 5B). Notably, RITC-labeled ESC-ABD alone was undetectable with the FOBI bioimaging system (at NIR mode), but the RITC-labeled ESC-ABD-AuNPs were visible (Supplementary Figure S1). This could be explained by the right shift of the fluorescence emission wavelength of the ESC-ABD-AuNPs. Conclusively, the fluorescence observed from the tissues by the FOBI bioimaging system shows only the intact ESC-ABD-AuNPs. Interestingly, some of the ESC-ABD-AuNPs could even be observed in the brain tissue, which suggested that it could be useful for drug delivery to the brain in further studies. However, before considering possible applications, it would be necessary to confirm which is the major factor that causes the brain delivery possible and also the potential capacity of the brain delivery amount.

After confirming the long-lasting properties of the ESC-ABD-AuNPs, their therapeutic efficacy was assessed through a single administration study and a long-term 4-week study in HFD-fed mice. In the single administration study, ESC-ABD-AuNPs demonstrated blood glucose-lowering effects comparable to ESC-ABD even administered by s.c. injection (Figure 6A). Compared with the i.v. route, the s.c. route is less painful, requires less professional injection skills (available for self-medication by patients), and allows greater injection volume.[37] However, if the molecule (or particle) size is too large, the absorption into the vessels could be severely impeded.[37] Because of this size issue, the particles are usually not injected via s.c. route.[38–40] However, interestingly and notably, in our study, even the ESC-ABD-AuNPs were injected via s.c. route, equivalent therapeutic effects were observed; suggesting sufficient absorption was available. Consistently, in the long-term study, the ESC-ABD-AuNPs exhibited equivalent effects to the ESC-ABD in reducing body weights (Figure 6D) and blood glucose levels (Figure 6C) and improving glucose tolerance (Figure 6E).

When the 4-week study was terminated, the liver and pancreas were harvested for further analysis. H&E staining of pancreatic sections revealed that the control group exhibited enlarged pancreatic islets (Figure 6G). This enlargement is consistent with previous reports, which suggest that, in hyperglycemic conditions, β-cells undergo hypertrophy to compensate for the heightened insulin demand.[41,42] Prolonged stress on β-cells can eventually lead to exhaustion and permanent damage.[43,44] Notably, treatment with ESC-ABD-AuNPs appeared to reverse this condition, as shown in Figure 6G and H, potentially normalizing pancreatic islet size and promoting insulin homeostasis.

The liver serves as a crucial metabolic hub, managing a variety of nutrients. While not a normal site for fat storage, it continuously exchanges free fatty acids (FFAs) with other tissues.[45,46] Instead of accumulating in the liver, FFAs are typically metabolized via β-oxidation in the mitochondria or converted into triglycerides (TGs) and very low-density lipoproteins (VLDL) for transport into the bloodstream.[46–48] This mechanism allows the liver to efficiently regulate FFAs

and prevent excessive buildup. However, in NAFLD, lipid droplets accumulate in liver cells, marking a key feature of the condition.[49] Fat accumulation results from an imbalance between FFA production and disposal, leading to the buildup of TGs and FFAs.[50–52] This triggers oxidative stress, mitochondrial dysfunction, and endoplasmic reticulum (ER) stress, ultimately causing liver cell damage.[53–55] The ESC-ABD-AuNPs treatment demonstrated a promising effect in the management of NAFLD. When compared to the control group, treatments with both ESC-ABD and ESC-ABD-AuNPs led to a notable reduction in liver size (Figure 7A) and liver weight (Figure 7B). Histological analysis further supported these findings. In the control group, liver tissues stained with H&E and Nile Red revealed a substantial buildup of intracellular lipid droplets, a hallmark of NAFLD. However, in the groups treated with ESC-ABD and ESC-ABD-AuNPs, there was a significant reduction in the number and size of lipid droplets (Figure 7C and D). This demonstrates the ability of these samples to mitigate fat accumulation in the liver, a critical step in preventing the disease from progressing to more severe conditions such as NASH.[56–58] Beyond these morphological improvements, treatments also led to better liver function, as indicated by decreased levels of AST and ALT—biomarkers commonly elevated in liver damage (Figure 7F and G).[59] Lower levels of AST and ALT suggest that both ESC-ABD and ESC-ABD-AuNPs treatments helped protect liver cells from injury, further underscoring their potential in NAFLD therapy.[60]

Another goal of the study was to prove the potential of the ESC-ABD-AuNPs as a delivery vehicle for therapeutics for the combination therapy of NAFLD. OCA, a small molecule FXR agonist, is currently in Phase 3 clinical trials for NAFLD and related conditions (NCT03439254). In this study, we investigated the feasibility of loading OCA onto the ESC-ABD-AuNPs. According to the loading study results (Figure 3E), the loading efficiency of OCA could be up to 3.6%; suggesting that the ESC-ABD-AuNPs could be a carrier for combination therapies with co-delivery of protein and small molecule drugs. Overall, through all the studies, the ESC-ABD-AuNPs were found to possess significant potential to become effective nanotherapeutics for NAFLD.

Conclusion

Here, ESC-ABD-AuNPs were successfully synthesized by a simple 1-step reduction process. These NPs demonstrated an extended plasma half-life and selective accumulation in the liver. Notably, the ESC-ABD-AuNPs showed significant and prolonged hypoglycemic and anti-NAFLD effects equivalent to ESC-ABD, even via s.c. injection. Furthermore, loading small molecules (eg, OCA) to the particles were found to be available, suggesting a potential use for combination therapy. Overall, this research demonstrated that the ESC-ABD-AuNPs hold promise as nanotherapeutics for NAFLD and further as an efficient carrier for combination therapies, potentially enhancing the NAFLD treatment outcomes. However, immunogenicity concerns are yet to be resolved for consideration of clinical use.

Ethics Approval and Informed Consent

Animal experiments were approved by the GNU's Committee for Animal Research (GNU-230615-M0131). All the animal studies were conducted in compliance with the National Institute of Health Guidelines on the Use of Laboratory Animals.

Acknowledgment

The authors thank Jaewoog Lee and Hyun Joo Shin for their contributions to the analysis and experimental support. They provided help for glucose-dependent insulin release study and nile red staining experiments.

Funding

This work was financially supported by the National Research Foundation of Korea (NRF) grant funded by the Korean government (MSIT; Ministry of Science and ICT) (NRF-2021R1F1A1058214 to M.C.S., NRF-2021R1F1A1064206 to K.A.M.). This study was also supported by the grant from Basic Science Research Program through the National Research Foundation of Korea (No. RS-2023-00219399) to M.C.S and G.S.R.

Disclosure

The authors report no conflicts of interest in this work.

References

1. Cotter TG, Rinella M. Nonalcoholic fatty liver disease 2020: the state of the disease. *Gastroenterol*. 2020;158(7):1851–1864.
2. Brunt EM, Wong VW-S, Nobili V, et al. Nonalcoholic fatty liver disease. *Nat Rev Dis Primers*. 2015;1(1):1–22.
3. Marchisello S, Di Pino A, Scicali R, et al. Pathophysiological, molecular and therapeutic issues of nonalcoholic fatty liver disease: an overview. *Int J mol Sci*. 2019;20(8):1948. doi:10.3390/ijms20081948
4. Friedman SL, Neuschwander-Tetri BA, Rinella M, Sanyal AJ. Mechanisms of NAFLD development and therapeutic strategies. *Nat Med*. 2018;24(7):908–922. doi:10.1038/s41591-018-0104-9
5. Boey A, Ho HK. All roads lead to the liver: metal nanoparticles and their implications for liver health. *Small*. 2020;16(21):2000153. doi:10.1002/smll.202000153
6. Sadauskas E, Wallin H, Stoltenberg M, et al. Kupffer cells are central in the removal of nanoparticles from the organism. *Part Fibre Toxicol*. 2007;4:1–7. doi:10.1186/1743-8977-4-10
7. Amendola V, Pilot R, Frasconi M, Maragò OM, Iatì MA. Surface plasmon resonance in gold nanoparticles: a review. *J Phys*. 2017;29(20):203002. doi:10.1088/1361-648X/aa60f3
8. Lyu Y, Becerril LM, Vanzan M, et al. The interaction of amines with gold nanoparticles. *Adv Mater*. 2024;36(10):2211624. doi:10.1002/adma.202211624
9. Min-Xuan X, Wang M, Wei-Wei Y. Gold-quercetin nanoparticles prevent metabolic endotoxemia-induced kidney injury by regulating TLR4/NF-kB signaling and Nrf2 pathway in high fat diet fed mice. *I J Nanomed*. 2017;12:327. doi:10.2147/IJN.S116010
10. Dkhil MA, Bauomy AA, Diab MS, Al-Quraishy S. Antioxidant and hepatoprotective role of gold nanoparticles against murine hepatic schistosomiasis. *Int J Nanomed*. 2015;10:7467–7475.
11. Conlon JM, Mechkarska M, Coquet L, et al. Characterization of antimicrobial peptides in skin secretions from discrete populations of Lithobates *chiricahuensis* (Ranidae) from central and southern Arizona. *Peptides*. 2011;32(4):664–669. doi:10.1016/j.peptides.2011.01.018
12. Pantic JM, Jovanovic IP, Radosavljevic GD, et al. The potential of frog skin-derived peptides for development into therapeutically-valuable immunomodulatory agents. *Molecules*. 2017;22(12):2071. doi:10.3390/molecules22122071
13. Amatya R, Park T, Hwang S, et al. Drug delivery strategies for enhancing the therapeutic efficacy of toxin-derived anti-diabetic peptides. *Toxins*. 2020;12(5):313.
14. Conlon JM, Mechkarska M, Abdel-Wahab YH, Flatt PR. Peptides from frog skin with potential for development into agents for Type 2 diabetes therapy. *Peptides*. 2018;100:275–281.
15. Ojo OO, Srinivasan DK, Owolabi BO, et al. Esculentin-2CHa-related peptides modulate islet cell function and improve glucose tolerance in mice with diet-induced obesity and insulin resistance. *PLoS One*. 2015;10(10):e0141549. doi:10.1371/journal.pone.0141549
16. Vasu S, McGahon MK, Moffett RC, et al. Esculentin-2CHa (1-30) and its analogues: stability and mechanisms of insulinotropic action. *J Endocrinol*. 2017;232(3):423–435. doi:10.1530/JOE-16-0453
17. Vasu S, Ojo OO, Moffett RC, et al. Anti-diabetic actions of esculentin-2CHa (1–30) and its stable analogues in a diet-induced model of obesity-diabetes. *Amino Acids*. 2017;49:1705–1717.
18. Lee J, Amatya R, Kim KE, et al. Genetically engineered long-acting Esculentin-2CHa (1− 30) fusion protein with potential applicability for the treatment of NAFLD. *J Control Release*. 2024;372:699–712. doi:10.1016/j.jconrel.2024.06.061
19. Ryu GR, Bae D, Uddin S, et al. Effect of transcription factor MEOX on insulin gene expression in glucagon-like peptide 1-secreting cells. *Vitro Cell Dev Biol Anim*. 2024;60(9):1099–1108. doi:10.1007/s11626-024-00964-6
20. Ryu GR, Lee E, Kim JJ, et al. Comparison of enteroendocrine cells and pancreatic β-cells using gene expression profiling and insulin gene methylation. *PLoS One*. 2018;13(10):e0206401.
21. Haiss W, Thanh NT, Aveyard J, Fernig DG. Determination of size and concentration of gold nanoparticles from UV− Vis spectra. *Analyt Chem*. 2007;79(11):4215–4221.
22. Petros RA, DeSimone JM. Strategies in the design of nanoparticles for therapeutic applications. *Nat Rev Drug Discov*. 2010;9(8):615–627.
23. Zeb A, Gul M, T-T-L N, Maeng H-J. Recent progress and drug delivery applications of surface-functionalized inorganic nanoparticles in cancer therapy. *J Pharm Investig*. 2023;53(6):743–779.
24. Shim G, Jeong S, Oh JL, Kang Y. Lipid-based nanoparticles for photosensitive drug delivery systems. *J Pharm Investig*. 2022;52:151–160. doi:10.1007/s40005-021-00553-9
25. Wang AZ, Gu F, Zhang L, et al. Biofunctionalized targeted nanoparticles for therapeutic applications. *Expert Opin Biol Ther*. 2008;8(8):1063–1070. doi:10.1517/14712598.8.8.1063
26. Lee KX, Shameli K, Yew YP, et al. Recent developments in the facile bio-synthesis of gold nanoparticles (AuNPs) and their biomedical applications. *Int J Nanomed*. 2020;Volume 15:275–300. doi:10.2147/IJN.S233789
27. Hassan H, Sharma P, Hasan MR, et al. Gold nanomaterials–The golden approach from synthesis to applications. *Mater Sci Energy Technol*. 2022;5:375–390.
28. Pelaz B, Del Pino P. Synthesis applications of gold nanoparticles. In *Frontiers of Nanoscience*. 2012;3–33.
29. Turkevich J, Stevenson PC, Hillier J. A study of the nucleation and growth processes in the synthesis of colloidal gold. *Discuss Faraday Soc*. 1951;11:55–75.
30. Xu M, Qi Y, Liu G, et al. Size-dependent in vivo transport of nanoparticles: implications for delivery, targeting, and clearance. *ACS Nano*. 2023;17(21):20825–20849. doi:10.1021/acsnano.3c05853
31. Haripriyaa M, Suthindhiran K. Pharmacokinetics of nanoparticles: current knowledge, future directions and its implications in drug delivery. *Future J Pharm Sci*. 2023;9(1):113. doi:10.1186/s43094-023-00569-y
32. Zhao Y, Sultan D, Liu Y. Biodistribution, excretion, and toxicity of nanoparticles. In *Theranostic Bionanomaterials*. 2019;27–53.
33. Poisson J, Lemoinne S, Boulanger C, et al. Liver sinusoidal endothelial cells: physiology and role in liver diseases. *J Hepatol*. 2017;66(1):212–227. doi:10.1016/j.jhep.2016.07.009
34. Bhandari S, Larsen AK, McCourt P, Smedsrød B, Sørensen KK. The scavenger function of liver sinusoidal endothelial cells in health and disease. *Front Physiol*. 2021;12:757469. doi:10.3389/fphys.2021.757469

35. Park J-K, Utsumi T, Seo Y-E, et al. Cellular distribution of injected PLGA-nanoparticles in the liver. *Nanomedicine*. 2016;12(5):1365–1374. doi:10.1016/j.nano.2016.01.013
36. Amatya R, Lee D, Min KA, Shin MC. Pharmaceutical strategies to improve druggability of potential drug candidates in nonalcoholic fatty liver disease therapy. *Pharmaceutics*. 2023;15(7):1963. doi:10.3390/pharmaceutics15071963
37. Usach I, Martinez R, Festini T, Peris J-E. Subcutaneous injection of drugs: literature review of factors influencing pain sensation at the injection site. *Adv Ther*. 2019;36:2986–2996. doi:10.1007/s12325-019-01101-6
38. Zhang LF, Deng WQ, Huang QW, et al. Vicious cycle-breaking lipid nanoparticles remodeling multicellular crosstalk to reverse liver fibrosis. *Adv Mater*. 2024;36(16):2311474. doi:10.1002/adma.202311474
39. Carvajal S, Perramón M, Oró D, et al. Cerium oxide nanoparticles display antilipogenic effect in rats with non-alcoholic fatty liver disease. *Sci Rep*. 2019;9(1):12848. doi:10.1038/s41598-019-49262-2
40. Zeng J, Acin-Perez R, Assali EA, et al. Restoration of lysosomal acidification rescues autophagy and metabolic dysfunction in non-alcoholic fatty liver disease. *Nat Commun*. 2023;14(1):2573. doi:10.1038/s41467-023-38165-6
41. Rathwa N, Patel R, Palit SP, et al. β-cell replenishment: possible curative approaches for diabetes mellitus. *Nutr, Metab Cardiovasc Dis*. 2020;30 (11):1870–1881. doi:10.1016/j.numecd.2020.08.006
42. Collares-Buzato CB. High-fat diets and β-cell dysfunction: molecular aspects. In Molecular Nutrition and Diabetes. 2016;115–130.
43. Prentki M, Peyot M-L, Masiello P, Madiraju SM. Nutrient-induced metabolic stress, adaptation, detoxification, and toxicity in the pancreatic β-cell. *Diabetes*. 2020;69(3):279–290. doi:10.2337/dbi19-0014
44. Fonseca SG, Burcin M, Gromada J, Urano F. Endoplasmic reticulum stress in β-cells and development of diabetes. *Curr Opin Pharmacol*. 2009;9 (6):763–770. doi:10.1016/j.coph.2009.07.003
45. Carotti S, Aquilano K, Valentini F, et al. An overview of deregulated lipid metabolism in nonalcoholic fatty liver disease with special focus on lysosomal acid lipase. *Am J Physiol Gastrointest Liver Physiol*. 2020;319(4):G469–G480. doi:10.1152/ajpgi.00049.2020
46. Morio B, Panthu B, Bassot A, Rieusset J. Role of mitochondria in liver metabolic health and diseases. *Cell Calcium*. 2021;94:102336. doi:10.1016/j.ceca.2020.102336
47. Geng Y, Faber KN, de Meijer VE, Blokzijl H, Moshage H. How does hepatic lipid accumulation lead to lipotoxicity in non-alcoholic fatty liver disease? *Hepatol Int*. 2021;15:21–35. doi:10.1007/s12072-020-10121-2
48. Berlanga A, Guiu-Jurado E, Porras JA, Auguet T. Molecular pathways in non-alcoholic fatty liver disease. *Clin Exp Gastroenterol*. 2014;7:221–239. doi:10.2147/CEG.S62831
49. Mashek DG. Hepatic lipid droplets: a balancing act between energy storage and metabolic dysfunction in NAFLD. *mol Metab*. 2021;50:101115. doi:10.1016/j.molmet.2020.101115
50. Bessone F, Razori MV, Roma MG. Molecular pathways of nonalcoholic fatty liver disease development and progression. *Cell mol Life Sci*. 2019;76:99–128. doi:10.1007/s00018-018-2947-0
51. Sahini N, Borlak J. Recent insights into the molecular pathophysiology of lipid droplet formation in hepatocytes. *Prog Lipid Res*. 2014;54:86–112. doi:10.1016/j.plipres.2014.02.002
52. Gowda D, Shekhar C, Gowda B, Chen SG, Y HS-P. Crosstalk between lipids and non-alcoholic fatty liver disease. *Livers*. 2023;3(4):687–708. doi:10.3390/livers3040045
53. Yuzefovych LV, Musiyenko SI, Wilson GL, Rachek LI. Mitochondrial DNA damage and dysfunction, and oxidative stress are associated with endoplasmic reticulum stress, protein degradation and apoptosis in high fat diet-induced insulin resistance mice. *PLoS One*. 2013;8(1):e54059. doi:10.1371/journal.pone.0054059
54. Ashraf N, Sheikh T. Endoplasmic reticulum stress and oxidative stress in the pathogenesis of non-alcoholic fatty liver disease. *Free Radical Res*. 2015;49(12):1405–1418. doi:10.3109/10715762.2015.1078461
55. Paradies G, Paradies V, Ruggiero FM, Petrosillo G. Oxidative stress, cardiolipin and mitochondrial dysfunction in nonalcoholic fatty liver disease. *World J Gastroenterol*. 2014;20(39):14205. doi:10.3748/wjg.v20.i39.14205
56. Pierantonelli I, Svegliati-Baroni G. Nonalcoholic fatty liver disease: basic pathogenetic mechanisms in the progression from NAFLD to NASH. *Transplantation*. 2019;103(1):e1–e13. doi:10.1097/TP.0000000000002480
57. Marra F, Lotersztajn S. Pathophysiology of NASH: perspectives for a targeted treatment. *Curr Pharm Design*. 2013;19(29):5250–5269. doi:10.2174/13816128113199990344
58. Takaki A, Kawai D, Yamamoto K. Molecular mechanisms and new treatment strategies for non-alcoholic steatohepatitis (NASH). *Int J mol Sci*. 2014;15(5):7352–7379. doi:10.3390/ijms15057352
59. Zhang W, Hong R, Tian T. Silymarin's protective effects and possible mechanisms on alcoholic fatty liver for rats. *Biomol Ther*. 2013;21(4):264. doi:10.4062/biomolther.2013.020
60. Duvnjak M, Tomasic V, Gomercic M, et al. Therapy of nonalcoholic fatty liver disease: current status. *J Physiol Pharmacol*. 2009;60(Suppl 7):57–66.